Sustainable Environment Research

RESEARCH

Open Access

The long-term effect of SiO_2 nanoparticles in drinking water inducing chronic kidney disease in a mouse model with modern dietary habits

Tzung Cheng Ye[1], Shu-Ju Chao[1] and Chihpin Huang[1*]

Abstract

SiO_2 nanoparticles (SNPs), which reportedly have low potential side effects, are used in various applications, for example, as food additives, for drug delivery, and as semiconductors, but these NPs are a growing concern because a few studies have shown potential risks to human health, such as fatty liver formation. In recent years, dietary habits have changed, and more refined foods, sugary beverages, and fast food are being increasingly consumed during daily life; therefore, the dietary habits have changed toward increasing consumption of high-fat diets, which may increase the incidence of liver and kidney disease. Our in vivo study demonstrated that the administration of SNPs in drinking water in combination with a high-fat diet was associated with the accumulation of SNPs and triglycerides in renal tissue; elevations in the blood urea nitrogen, uric acid, and creatinine levels in serum; the formation of basophilia and tubular cell sloughing; abnormal renal parenchyma, cysts, and hyaline casts; the induction of proliferating cell nuclear antigen and markers for chronic kidney disease such as vimentin, lipocalin 2, kidney injury molecule; the activation of fibrosis and inflammation; increased oxidative stress; and the development of chronic kidney disease. The evidence showed that long-term treatment of SNPs in drinking water might induce renal injury in individuals with modern dietary habits and provided important results for evaluating the safety of SNPs, especially for human health.

Keywords Drinking water, High-fat diet, Normal diet, Nanoparticles, Chronic kidney disease

1 Introduction

Obesity, which usually results from modern dietary habits, has been recognized as an independent and important factor in the development of chronic kidney disease (CKD) [1]. Obesity, a component of metabolic syndrome, is often observed in patients with hyperglycemia, diabetes, and cardiovascular disease, among other diseases [2]. A chronic inflammatory state not only is induced by many adipokines, cytokines, and chemokines due to the accumulation of triacylglycerols (TGs) but also affects insulin resistance, which contributes to the release of free fatty acids in the blood and free fatty acids cause lipotoxicity to tissues such as the liver and kidney [3]. The kidney, which contains very small filter glomeruli in each nephron, has the major function of removing waste, for instance, urine, uric acid, and nitrogen waste. In chronic hyperlipidemic conditions, excess lipids accumulate and cause lipotoxicity, driving the activation of fibrosis, inflammation, apoptosis, and renal dysfunction [4, 5]. Renal lipid metabolism syndrome and oxidative stress

*Correspondence:
Chihpin Huang
huang@nycu.edu.tw
[1] Institute of Environmental Engineering, National Yang Ming Chiao Tung University, Hsinchu, Taiwan

have been found to induce lysosomal dysfunction and mitochondrial dysfunction, leading to kidney injury in mice fed a high-fat diet for a long time [6, 7].

Chronic kidney disease, also known as chronic renal failure, has influenced more than 10% of the world's population and is characterized by an unclear etiology and irreversible deterioration of renal capacity; however, factors such as sex, age, diet, and hormones may affect its occurrence. CKD is a common renal disease, especially in older and diabetic populations and in patients with hypertension. CKD causes glomerular and tubulointerstitial pathology, has degenerative and regenerative characteristics, and is usually age-dependent. Early lesions in the kidney exhibit tubular basophilia, basement membrane thickening, and infiltration by immune cells. With the progression of CKD, an increase in the number of abnormal renal parenchyma, prominent hyaline casts, and an increase in the incidence of proliferative lesions are found in the kidney. When the glomerular filtration rate decreases, CKD may progress to the end-stage kidney and subsequently cause death. However, the finding that nanoparticles (NP) and toxicants, such as SiO_2 NP (SNPs) and heavy metals, could contribute to CKD pathogenesis and that exposure can occur through ingestion, such as from contaminated drinking water, are concerns [8, 9].

Although the turbidity of drinking water must be lower than 2 NTU according to most drinking water regulations, drinking water still contains many NPs, such as SNPs [10]. SNPs are the most common inorganic NPs and are widely used in different industries, such as biomedicine, agriculture, and cosmetics. In vivo and in vitro effects of SNPs include cellular cytotoxicity, reactive oxidative stress, induction of apoptosis, mitochondrial and DNA damage, abnormal hepatocyte morphology, lipid metabolism dysfunction, oxidative stress, fibrosis, and inflammation [11–17]. SNPs may accumulate in major organs such as the liver, kidney, and lung and induce hepatic steatosis, renal disease, and pulmonary fibrosis [18–20]. Global hypoacetylation, which is induced by SNPs, results in global epigenomic activity through decreases in the mRNA and protein levels of methyltransferases and DNA-binding proteins [21]. cDNA microarray and proteomic studies have shown that SNPs can affect inflammation-related gene expression via alterations in chemokines and cytokines, apoptosis, the transcription and translation of regulatory genes, and oxidative stress [22, 23]. Therefore, due to the rapid development and use of nanotechnology products, the gradually increasing use of amorphous SNPs in commercial products, such as cosmetics and toothpaste, has increased human exposure to SNPs and the potential risk to human health [24]. In India, CKD has been linked to groundwater, which is exposed to silica [25]. Northern Sri Lanka, which contains a CKD-related endemic area, also has high levels of silica in its groundwater [26]. The oral administration of silica is reportedly associated with renal lesions in rats [27]. Thus, the toxicity of silica remains a potential factor in CKD. However, fewer studies have focused on the combined long-term effects of SNPs and modern dietary habits, both of which are associated with lipid metabolism dysfunction.

To understand the correlation between SNPs and modern dietary habits, we used Institute of Cancer Research (ICR) mice, which are highly similar in genetics to *Homo sapiens*. To establish our ICR mouse model, mice were administered either a normal diet (ND) or a high-fat diet (HFD) with different concentrations of SNPs by oral gavage for 25 weeks to mimic long-term exposure to drinking water. Histology observation, analyses of the accumulation of silicon and TG in tissue, blood biochemical assays, picrosirius red/Masson trichrome staining, and immunohistochemical staining were used to determine the correlation between SNPs in drinking water and modern dietary habits in our model. This study investigated the interactions between environmental NPs, such as the long-term risk of exposure to SNPs, and dietary factors, suggesting a significant risk to human health.

2 Materials and methods

2.1 Preparation and properties of SiO_2 NPs

Stock solutions of the 40-nm amorphous SNPs (UniRegion Bio-Tech) were freshly prepared in reverse osmosis water and sterilized by autoclaving at 121 ℃ for 15 min prior to administration via oral gavage to our animal model. The morphology of the NPs was determined via by field emission transmission electron microscopy (TEM) (JELO, JEM-F200) at the National Yang-Ming Chiao Tung University Instrument Resource Center. ImageJ software (National Institutes of Health, Bethesda, MD, USA) was used to measure the size of the NPs. The hydrodynamic sizes and zeta potentials of the NPs in reverse osmosis media were analyzed using a Zetasizer Nano series instrument (Malvern, UK). The purity and endotoxin levels were determined by an Agilent inductively coupled plasma atomic emission spectrometer (Agilent 720, USA) and a gel-clot limulus amebocyte lysate assay, respectively.

2.2 Animal model

Male ICR mice, aged eight weeks and weighing 20–26 g, were purchased from BioLASCO Taiwan Co. All the mice were housed under conditions of 21 ± 2 ℃, 55 ~ 60% humidity, and a 12 h light–dark cycle. The animals were fed ad libitum either an ND (AIN-93G Diet, BioLASCO Taiwan Co.) providing 16.7% of the calories from fat, or

an HFD (high-fat AIN-93G purified Rodent Diet, BioLASCO Taiwan Co.) providing 52.4% of the calories from fat. The ICR mice were fed twice per week with different concentrations of the SNP stock media (suspended by vibration for 3 min) and separated into six groups ($n=6$ per group): (1) ND-SNP0, ICR mice fed the ND and given reverse osmosis water by oral gavage; (2) ND-SNP100, ICR mice fed the ND and treated with 100 mg of SNPs kg^{-1} mouse body weight by oral gavage (100 mg kg^{-1}); (3) ND-SNP300, ICR mice fed the ND and treated with 300 mg of SNPs kg^{-1} of mouse body weight by oral gavage (300 mg kg^{-1}); (4) HFD-SNP0, ICR mice fed the HFD and given reverse osmosis water by oral gavage; (5) HFD-SNP100, ICR mice fed the HFD and treated with 100 mg of SNPs kg^{-1} mouse body weight by oral gavage (100 mg kg^{-1}); and (6) HFD-SNP300, ICR mice fed the HFD and treated with 300 mg of SNPs kg^{-1} of mouse body weight by oral gavage (300 mg kg^{-1}). When choosing the SNP administration method, we opted for oral gavage instead of a water bottle for drinking because SNP precipitation easily occurs in reverse osmosis water. Therefore, we cannot accurately predict the intake of SNPs based on the amount of drinking water. According to previous studies, average concentrations of SNP administered to mice that did not exhibit abnormal behavior or have no obvious macroscopic effects ranged from 1.0 to 333 mg SNP kg^{-1} mouse body weight [18, 28–30], even at very high doses (1–2.5 g kg^{-1} body weight/day) [31, 32]. The total amount of silica we administered per week was below the maximum metabolic cycle of the mice and the best-tolerated mice. Therefore, we selected SNP therapeutic concentrations ranging from 100 to 300 mg kg^{-1} mouse body weight for long-term treatment. To understand the long-term effects of SNPs, we chose 100 and 300 mg of SNPs kg^{-1} of mouse body weight that were different from the real SNP concentration in drinking water for the experiment design. The mice were sacrificed under 4% isoflurane anesthesia via a gas anesthesia machine. Blood obtained by heart puncture and kidney tissue were collected from the mice continuously exposed to SNPs for 25 weeks. Blood and kidney organs fixed with 10% formalin were subjected to further blood biochemical assays, histopathological examinations, measurements of silicon in the kidney, and immunohistochemistry (IHC) at the Taiwan Mouse Clinic.

2.3 Serum preparation and blood biochemical assays

The blood was transferred to a BD microtainer[1] (BD, 365967 Gold BD SST™). Blood clotting was allowed to occur at room temperature for 20–30 min but not longer than 3 h to avoid hemolysis. Serum was obtained by the centrifugation of whole blood at 3,000 rpm for 15 min at 4 ℃. The supernatant was transferred to a new 1.5 mL Eppendorf tube, and the serum was stored at -80 ℃ for future experiments. 10 µL of serum were directly used for the analysis of various kidney function-related biomarkers, such as alanine aminotransferase (ALT), aspartate aminotransferase (AST), blood urea nitrogen (BUN), uric acid (UA), creatinine (CRE) and C-reactive protein (CRP), with a biochemical analyzer (HITACHI 3100 analyzer, Japan).

2.4 Histopathological examination

The removed kidney tissues were fixed in 10% formalin, embedded in paraffin, sectioned, stained with hematoxylin and eosin (H&E) for histological examination by the Taiwan Mouse Clinic. After H&E staining, the slides were consulted by a nephrologist from the Taiwan Mouse Clinic and were observed and photographed with an optical microscope (Nikon, ECLIPSE Ci).

2.5 Silicon element accumulation in kidney tissue

The kidney tissues were homogenized in liquid nitrogen, and 0.5 g of homogenized kidney tissue was digested with 5 mL of hydrofluoric acid (Sigma, 7664–39-3) at 80 ℃ for 30 min. After digestion, the cooled sample was incubated with 1 mL of 30% hydrogen peroxide (Fluka-Honeywell, 31642) for complete oxidation at 80 ℃ for 30 min. The completely oxidized sample was cooled at room temperature and filtered through a 0.45-µm filter. The silicon concentration was analyzed using inductively coupled plasma (ICP) (Agilent Technologies ICP-OES 700 Series) at the National Yang-Ming Chiao Tung University Environment Technology & Smart System Research System.

2.6 Accumulated triglycerides in kidney tissue

A lipid extraction kit (BioVision, K216-50) was used for the extraction of TGs from kidney tissue. Kidney tissue (0.5 g) was mixed with 500 µL of lipid extraction buffer and homogenized on ice. The supernatant was left open and dried in an incubator at 37 ℃, and the lipid extract was then resuspended in 50 µL of lipid suspension buffer. The lipid extract was sonicated for 10 min at 37 ℃ and used to measure the TG amount using an automated biochemical analyzer (HITACHI 3100 analyzer, Japan) at the Taiwan Mouse Clinic.

2.7 Quantitative reverse transcription polymerase chain reaction (RT-PCR)

Total RNA was extracted from mouse kidney tissue with TRI Reagent (Sigma-Aldrich), and the mRNA levels of vimentin (*Vim*), lipocalin 2 (*Lcn2*), kidney injury molecule (*Kim-1*), and protein kinase, AMP-activated, alpha 1 catalytic subunit (*Prkaa1*) in mice kidneys were analyzed using SYBR Green-induced PCR through the CFX Opus Real-Time PCR system (Bio-Rad). Relative

mRNA expression was calculated using the delta-delta C_t method to normalize the target gene mRNA to *Gapdh*.

The following primers were used: *Gapdh*, forward 5' –ACCCAGAAGACTGTGGATGG-3' and reverse 5' -GGATGCAGGGATGATGTTCT-3'; Vim, forward 5' -CTGCACGATGAAGAGATCCA -3' and reverse 5' -AGCCACGCTTTCATACTTGTTT -3'; *Lcn2*, forward 5' -GAAATATGCACAGGTATCCTC-3' and reverse 5' -GTAATTTTGAAGTATTGCTTGTTT-3'; *Kim-1*, forward 5' -CTGGAATGGCACTGTGACATCC-3' and reverse 5' -GCAGATGCCAACATAGAAGCCC-3'; and *Prkaa1*, forward 5' -GGTGTACGGAAGGCAAAATGGC-3' and reverse 5' -CAGGATTCTTCCTTCGTACA CGC -3' [33].

2.8 Observation of kidney fibrosis by picrosirius red stain or Masson's trichrome staining

Kidney paraffin sections were stained with a picrosirius red kit (Scy Tek, SRS25) or Masson's trichrome staining kit (Sigma-Aldrich, HT15) following the manufacturer's protocol for the assessment of kidney fibrosis. The paraffin sections were deparaffinized with xylene and a series of decreasing ethanol series. The specimen sections were incubated with picrosirius red solution or aniline blue solution for 60 min at room temperature, and the slides were washed with acetic acid solution and absolute alcohol. The slides were dehydrated, mounted, and evaluated using an optical microscope (Nikon, ECLIPSE Ci). To observe the degree of fibrosis in kidney tissue, the percentage of the positively stained area was analyzed using an optical microscope (Nikon, ECLIPSE Ci), and the Image-Pro software (Total-smart Technology Co., Taichung, Taiwan).

2.9 IHC

For IHC, 8–10 μm thick paraffin-embedded tissue samples were deparaffinized with xylene and a series of decreasing ethanol series. The hydrated sections were pretreated with a citric acid solution (10 mM Trisodium salt dihydrate pH 6.0, 0.5% Tween-20) for 8 min. For nonspecific blocking, the sections were incubated with peroxidase (Thermo Scientific, Catalog N0. 31487) for 10 min at room temperature. After blocking, the slides were incubated overnight with the primary antibodies against proliferating cell nuclear antigen (PCNA) at a dilution of 1:200 (Genetex, GTX100539), $p21^{Clip1}$ at a dilution of 1:200 (Genetex, GTX629543), 4-hydroxynonenal (4-HNE) at a dilution of 1:200 (Genetex, GTX01087), tumor necrosis factor-alpha (TNF-α) at a dilution of 1:200 (Genetex, GTX110520), transforming growth factor beta (TGF-β) at a dilution of 1:200 (Genetex, GTX110527), or interleukin 6 (IL-6) at a dilution of 1:200 (Genetex, GTX130023). Subsequently, the slides were incubated with the appropriate secondary antibody for 1 h at room temperature. A mounting medium was used to envelop the slides. To observe the staining pattern of kidney tissue, the percentage of the positively stained area was analyzed using an optical microscope (Nikon, ECLIPSE Ci) and the Image-Pro software (Total-smart Technology Co., Taichung, Taiwan).

2.10 Statistical analysis

The results are presented as the means ± standard errors of the mean and were analyzed using SigmaPlot v14.0 software (Systat Software Inc, Palo Alto, CA, USA). Two-way analysis of variance (ANOVA) was used for the assessment of the significance of the differences: *, $p < 0.05$, **, $p < 0.005$, and ***, $p < 0.001$.

3 Results and discussion

3.1 Characterization of the SiO_2 nanoparticles

As shown in Fig. S1, the morphology of the SNPs was amorphous and dispersed, with an average diameter of 39.7 ± 5.2 (mean ± standard error). The hydrodynamic sizes and zeta potentials of the SNP stock solutions in reverse osmosis water are presented in Table S1. In addition, the purity of the SNPs was 99.99%. Free endotoxin was detected in our SNP sample.

3.2 SNPs aggravated the body weight of mice fed with an ND or HFD, and silicon deposition in the kidney

Figure 1a shows the body weight variations in the ND- or HFD-fed ICR mice after the oral administration of different concentrations of SNPs. All mice tolerated twice weekly doses between 100 and 300 mg kg^{-1} administered oral gavage during the experimental period. The body weights of each group were slightly increased in a time-dependent manner. After 8 weeks of treatment, the body weights of the HFD-SNP0 group were significantly higher than those of the ND-SNP0 group ($p < 0.01$, ANOVA) (Fig. 1a). The results showed that the HFD led to an increase in body weight after 8 weeks of treatment because the HFD provided a higher caloric intake. Regardless of the diet, no significant differences in body weight were observed in ND and HFD groups. ($p > 0.05$, ANOVA) (Fig. 1a). During the experimental period, no abnormal behavior, such as labored breathing or arching of the back; no clinical signs, such as bloating and vomiting; and no apparent induced toxicity, were observed. After sacrifice at the end of the 25-week experimental period, no visible changes in organ morphology were

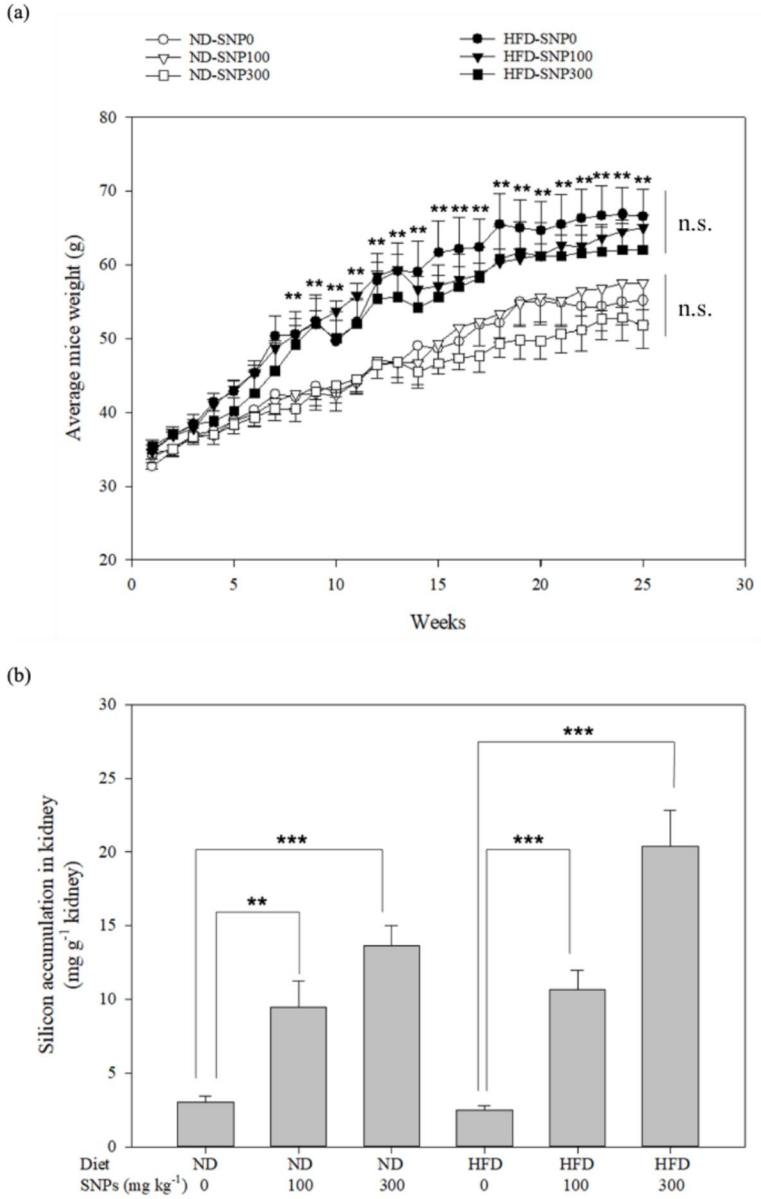

Fig. 1 Body weight changes in mice. Mice treated with 0, 100, or 300 mg kg^{-1} SNPs by oral gavage twice per week and fed an ND or HFD (**a**). Each point represents the mean ± standard error of the mean ($n = 6$). **, $p < 0.01$ for the comparison of the HFD-SNP0 group with the ND-SNP0 group, as revealed by ANOVA. Body weight differences were observed between the ND- and HFD-fed mice treated with different concentrations of SNPs ($p > 0.05$, ANOVA). No significance (n.s.). The accumulation of silicon in kidney tissue (mg of silicon per kidney gram) was measured at 25 weeks by ICP (**b**). The data are presented as the means ± standard errors of the means ($n = 6$)

detected. Therefore, the simulated SNPs had no immediate or noticeable impact on our mouse model.

ICP, a method used for quantifying specific elements present in samples, was used to analyze the average silicon accumulation (μg silicon g^{-1} kidney). The amount of silicon in the kidneys of mice in the ND-SNP100 and ND-SNP300 groups was significantly different from that in the ND-SNP0 group ($p < 0.001$–0.01, ANOVA), respectively (Fig. 1b). The silicon accumulation in the HFD groups significantly increased with increases in the SNP dose ($p < 0.001$–0.01, ANOVA) (Fig. 1b). Our results further demonstrated that SNPs might accumulate in the kidney and similarity, previous research has shown that silicon accumulates in kidney tissue [34].

Materials such as NPs can be taken up into the cells passing through the plasma membrane by endocytosis,

which engulfs the NPs, and the cell membrane invaginates these particles into the cell by forming an intracellular vesicle [35]. However, the NP uptake mechanism should be considered with caution because the cellular uptake mechanism depends on the particle size (e.g., isolated or aggregated particles), surface modification (e.g., hydrophilic functional group), surface charge, dosage, exposure time, treatment media (e.g., content in media), and cell type used as a model. According to this study, the silicon accumulated in the kidney, and we speculated that the SNPs might enter the kidney tissue through endocytosis. Not only the kidneys but also other organs, such as the liver and lungs, are the position in which SNP could accumulate [18–20]. However, the uptake of SNPs still has many unclear questions that need to be discussed in depth.

3.3 Blood biochemical parameter analyses of the serum of mice and TG expression in kidney tissue

Our study evaluated the levels of biochemical blood parameters, such as AST and ALT, in the serum of mice administered SNPs to determine the physical condition of the mice. At 25 weeks, the serum AST and ALT levels were higher in the HFD-SNP0 group than in the ND-SNP0 group ($p < 0.05$, ANOVA) (Fig. 2a and b), and no changes in the AST and ALT levels were observed in the ND-SNP100 or HFD-SNP100 groups compared with the ND-SNP0 or HFD-SNP0 groups, respectively ($p > 0.05$, ANOVA) (Fig. 2a and b). However, an increase in the AST level ($p < 0.05$, ANOVA), but no change in the ALT level ($p > 0.05$, ANOVA), was found in the ND-SNP300 group compared with the ND-SNP0 group (Fig. 2a and b). At 25 weeks, the HFD-SNP300 group has significantly higher serum levels of AST and ALT than the HFD-SNP0 group ($p < 0.01$–0.001, ANOVA) (Fig. 2a and b).

Based on its clinical significance and laboratory findings, AST is present in large amounts in the liver, heart, muscle, and other tissues and can be used to diagnose myocardial infarction, hepatobiliary disease, and muscle disorders [36–38]. Violent viral hepatitis, acute hepatitis, hepatocellular necrosis, alcoholic hepatitis, traumatic necrosis of the heart or skeletal muscles, and excessive exercise significantly increase the serum AST concentration [36–38]. However, an HFD not only induces fatty liver, obesity, and overweight but also promotes renal injury through oxidative stress and mitochondrial dysfunction [7]. In a 5/6 nephrectomized rat model, which has been used to study CKD, the AST and ALT levels are induced in CKD [39]. Previous studies have shown that inhaled SNPs could cause chronic kidney disease [34]. These data showed that the increased serum AST and ALT levels not only affect liver function but also may control kidney function [34, 36–39]. Therefore, we hypothesized that the kidney might be injured in our mice fed an HFD and administered SNPs.

To determine kidney function, various biochemical blood parameters, such as BUN, UA, and CRE, were measured in the serum of mice administered SNPs and fed an ND or an HFD to determine their kidney function. No significant change in the serum levels of BUN and CRE ($p > 0.05$, ANOVA) was detected in the ND-SNP100 or ND-SNP300 group compared with the ND-SNP0 group (Fig. 2c and e). Increased serum levels of BUN and CRE were found in the HFD-SNP100 and HFD-SNP300 groups compared with the HFD-SNP0 group ($p < 0.01$–0.001, ANOVA) (Fig. 2c and e). The serum UA concentration was higher in the ND-SNP300 or HFD-SNP300 group than in the ND-SNP0 or HFD-SNP0 group, respectively ($p < 0.05$–0.001, ANOVA) (Fig. 2d). To analyze the TG levels in kidney tissue, TGs were extracted from homogenous renal tissue and analyzed with an automated biochemical analyzer (HITACHI 3100 analyzer, Japan). The HFD-SNP0 group exhibited higher TG levels than the ND-SNP0 group ($p < 0.001$, ANOVA) (Fig. 2f). Similar results were also found in other studies [7]. Among the ND groups, the TG levels in tissue were greater in the ND-SNP300 group than in the ND-SNP0 group ($p < 0.05$, ANOVA) (Fig. 2f). Among the HFD-treated mice fed SNPs, the TG levels in kidney tissue were higher in the HFD-SNP300 group compared with the HFD-SNP0 group ($p < 0.001$, ANOVA) (Fig. 2f). The accumulated TG concentration was higher in the HFD-SNP300 group than in the ND-SNP300 group ($p < 0.001$, ANOVA) (Fig. 2f), which indicated that the increase in TG accumulation may be induced by the HFD.

Although estimated Glomerular filtration rate can be more useful than BUN and CRE to evaluate the function of the kidney, it is not possible to calculate [40, 41]. Therefore, we used BUN and CRE to estimate the renal function. The general blood parameters are BUN (normal range, 16–25 mg dL^{-1}) and CRE (normal range, 0.3–0.4 mg dL^{-1}) [42], which reflect the level of urinary toxins and the quality of renal function, respectively. BUN, which indicates possible kidney damage, can easily be filtered from the renal glomerulus due to its small size. In contrast to BUN, CRE is derived from muscle tissue metabolism. Although CRE is also excreted in urine, it is less affected by food intake. Notably, at the early stages of renal impairment, BUN and CRE are easily filtered and excreted from the renal glomerulus due to their small molecular sizes: in particular, renal tubules also have the ability to secrete and excrete BUN and CRE. Hence, neither BUN nor CRE are excreted at the early stage of renal disease until kidney function decreases to approximately one-third or less of its normal levels. In other words, once the serum CRE

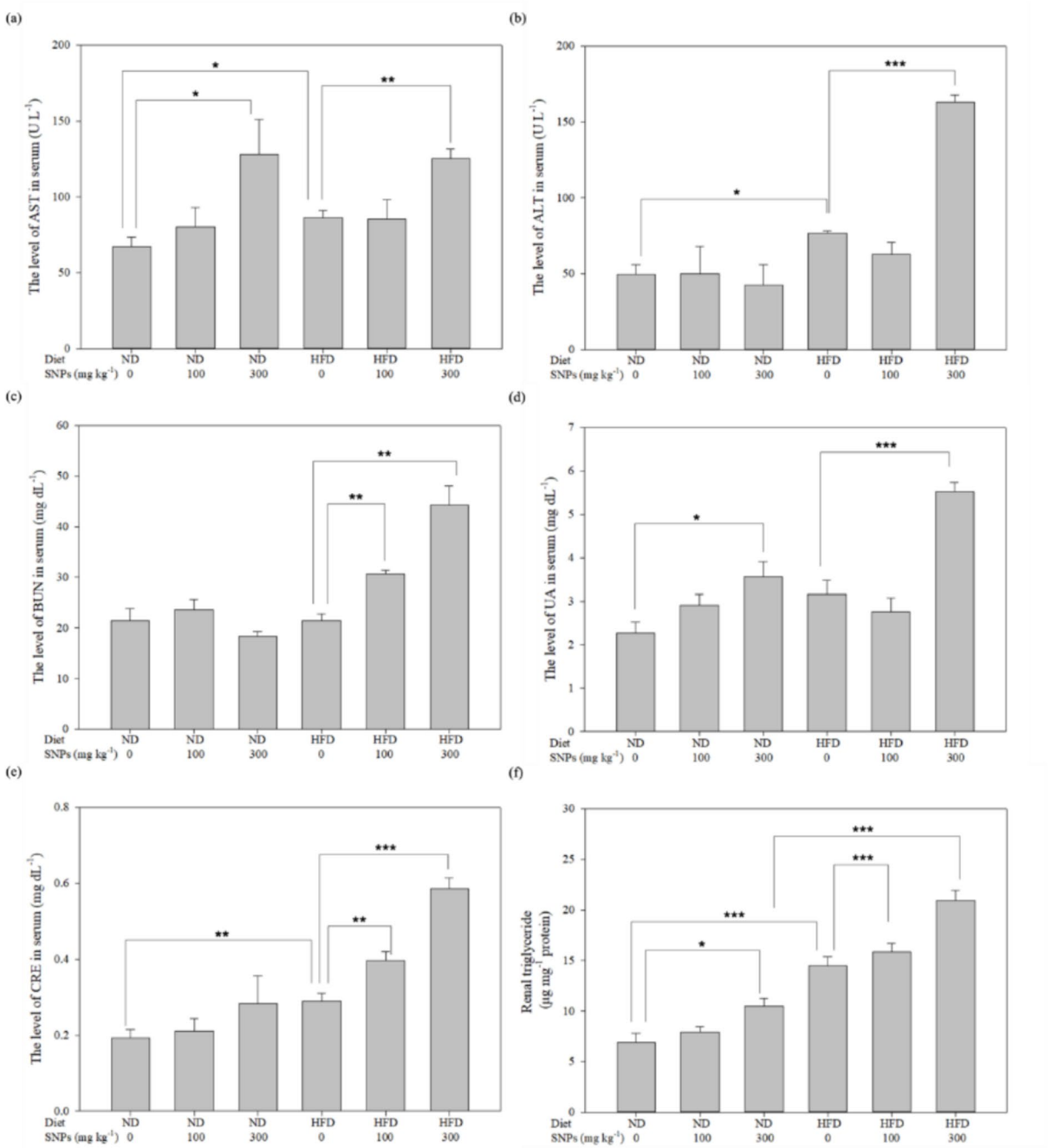

Fig. 2 The expression of blood biochemical markers in serum and TG in kidney tissue. Serum AST levels in U L^{-1} (**a**), ALT levels in U L^{-1} (**b**), BUN levels in mg dL^{-1} (**c**), UA levels in mg dL^{-1} (**d**), CRE levels in mg dL^{-1} (**e**), and accumulated TG levels (μg mg^{-1} protein) (**f**) in kidney tissue induced by treatment with SiO_2 nanoparticles in the ND and HFD groups at 25 weeks. The data are expressed as the means ± standard errors of the means ($n = 6$). No significance (n.s.)

level increases to an abnormal level, an expert should be consulted for further inspection and confirmation. Consistently, our data showed that the elevated serum levels of BUN and CRE were strongly associated with kidney disease in our mice fed an HFD and SNPs. To illustrate the development of kidney disease in our model, the morphology of the kidney and CKD markers were confirmed by H&E staining and quantitative RT-PCR.

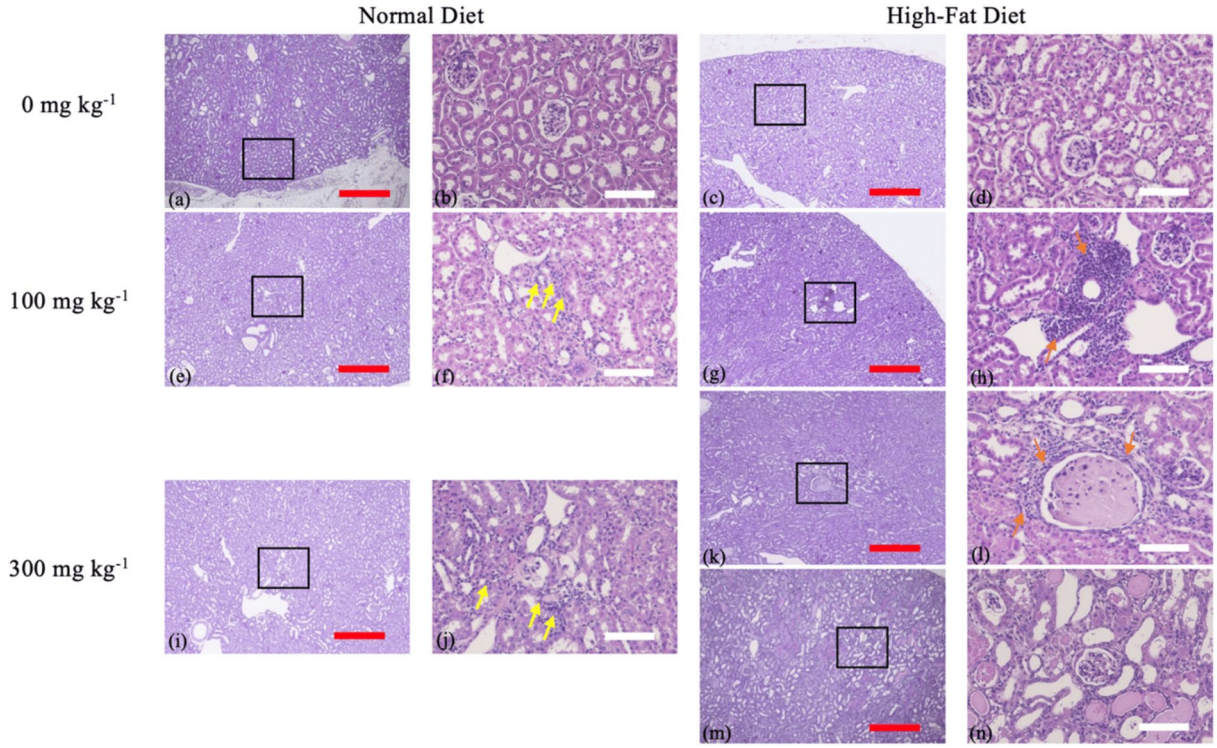

Fig. 3 The degree of CKD is shown by H&E staining. The mice were fed the ND (**a**, **b**, **e**, **f**, **i** and **j**) or HFD (**c**, **d**, **g**, **h**, **k**, **l**, **m** and **n**) for 25 weeks and treated with 0 (**a**, **b**, **c** and **d**), 100 (**e**, **f**, **g** and **h**), or 300 (**i**, **j**, **k**, **l**, **m** and **n**) mg kg^{-1} SNPs twice per week. The red scale bars represent 500 μm (**a**, **c**, **e**, **g**, **i**, **k** and **m**) and the white scale bars represent 100 μm (**b**, **d**, **f**, **h**, **j**, **l** and **n**). The yellow arrows indicate basophilia with a thickened basement membrane, and the orange arrows indicate immune cell infiltration

3.4 Induced CKD in a mouse model by SNPs and HFD

Figure 3a–d show the normal morphology of the kidney, which has a clear lumen space. In the ND-SNP100 and ND-SNP300 groups, we observed injured tubules (fragmented cytoplasm), basophilia, and tubular cell sloughing, which are the most common early signs of CKD; the results suggested that CKD might be induced by SNP treatment (Fig. 3e, f, i and j). Increased immune cell infiltration, which is characteristic of CKD, was found in the HFD-SNP100 and HFD-SNP300 groups (Fig. 3g, h, k and l). We also observed the cysts that arose from tubular dilation with homogenous eosinophilic fluid (Fig. 3k and l). Eosinophilic and homogeneous casts (prominent hyaline casts) and increasingly affected renal parenchyma, which are usually observed in advanced CKD (Fig. 3m and n), were observed in our mice fed the HFD and treated with 300 mg of SNPs kg^{-1} mouse body weight.

We carried out quantitative RT-PCR of vimentin (*Vim*), lipocalin 2 (*Lcn2*), and kidney injury molecular 1 (*Kim-1*) using RNA extracted from the mouse kidney. *Vim*, a marker for kidney fibrosis [43], and *Lcn2,* which also referred to neutrophil gelatinase-associated lipocalin and *Kim-1*, markers for tubular damage [44], increased significantly in our mice treated with SNPs with HFD ($p < 0.05$–0.001, ANOVA) (Fig. 4a–c).

Previous studies have shown that multifocal areas of basophilia and tubular cell sloughing can be observed at the early stage of CKD, and increased abnormal renal parenchyma, cysts, hyaline casts, and immune cell infiltration can be noted in the late-stage lesions [45]. The common markers such as *Vim*, *Lcn2*, and *Kim-1* were activated in CKD [43, 44]. It has been reported that AMPK plays a crucial role in renal cell dysfunction, and activating AMPK might improve kidney dysfunction [46–48]. Our results showed that the mRNA expression of *Prkaa1* (catalytic subunit in AMPK) decreased in SNPs and HFD treatment ($p < 0.01$, ANOVA) (Fig. 4d). Therefore, the mechanism of induced CKD might be through the AMPK pathway. Based on our experiment results, we hypothesized that the CKD induced in our mice treated with SNPs and the HFD would accelerate the development of CKD.

Long-term HFD feeding has been shown to induce lysosomal dysfunction and alter renal lipid metabolism, leading to renal injury [6, 49]. SNPs can induce chronic kidney disease [34]. The related research provides evidence showing that renal dysfunction may develop via

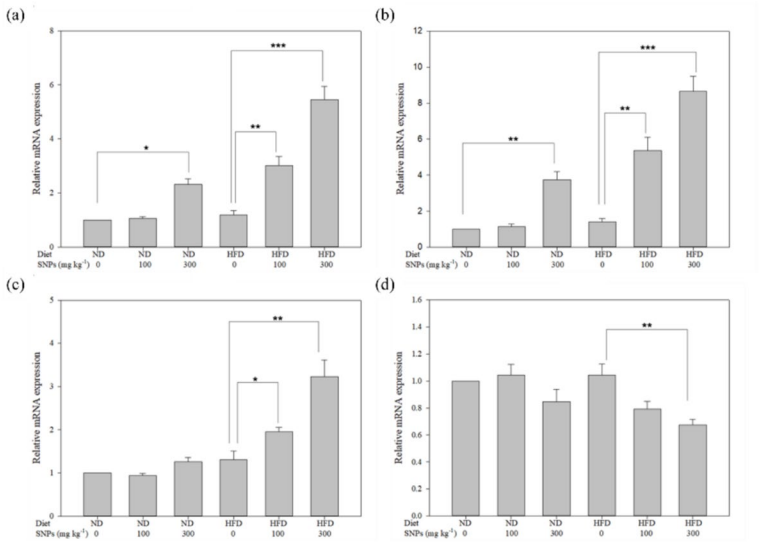

Fig. 4 Markers for CKD. Quantitative RT-PCR was used to analyze the kidney mRNA levels of *Vim* (**a**), *Lcn2* (**b**), *Kim-1* (**c**), and *prkaa1* (**d**) in mouse treatment with SNPs in the ND and HFD groups at 25 weeks. The data are expressed as the means ± standard errors of the means ($n = 6$)

stimulation through the combined effect of SNPs and HFD. Therefore, NPs such as SNPs and modern dietary habits are two important factors that affect human health.

In addition to histopathology, CKD is a regenerative and degenerative disease observed in autoradiographic and immunohistochemical cell proliferation studies and can cause chronic renal failure and death. The regenerative aspect of the process is supported by studies that examined PCNA expression [50]. PCNA expression peaks at the G1/S phase of interphase, and at this point, the protein is located mainly in the cell nucleus. PCNA is a potential marker for cells with proliferative potential and for identifying the proliferation status of tissue. Despite the increases in the incidence and severity of CKD with age, the evidence indicates that CKD should be regarded as a specific disease entity. To determine the aging effect of aging in our study, $p21^{Clip1}$, which is a marker of aging, was usually used to identify age-related diseases [51]. ND groups showed no positive immunohistochemical staining (Fig. 5a, c and e). Figure 5d and f show that the tubules of CKD mice were immunohistochemically stained for PCNA as a cell proliferation marker. The quantitative data also revealed the induction of regeneration in the HFD-SNP300 group compared with the HFD-SNP0 group ($p < 0.01$, ANOVA) (Fig. 5g). The results showed the presence of regenerative renal tissue in our mouse model, which was consistent with the findings of previous research. No signs of aging were detected by $p21^{Clip1}$ immunochemical staining (Figs. S2a–f) or quantitative analysis ($p > 0.05$, ANOVA) (Fig. S2g). Both sets of IHC staining results showed that regenerative CKD occurred after HFD and SNP treatment and may not occur due to aging.

3.5 Induction of IL-6 and TNF-α in HFD-fed mice administered SNPs

One of the hallmarks of CKD, which results in its development, progression, and complications, is continuous and low-grade inflammation. Inflammation, which occurs in response to different stimuli, is a necessary and normal body reaction. Immune cells that stimulate target sites, such as injury sites, can migrate to the target site following a series of steps facilitated and coordinated by cytokines, chemokines, and acute-phase proteins. In acute conditions, this process provides a resolution against human pathology. Chronic inflammation can lead to tissue damage and fibrosis formation. Therefore, inflammation has been associated with numerous diseases, including CKD and fatty liver disease [52]. Previous studies have shown that the cytokine markers of inflammation in CKD patients are interleukins, TNF, and TGF [53]. Cytokines play important effector and messenger roles in the development and activity of the immune system. Chronic inflammation, either due to inappropriate reactions against self-antigens or prolonged stimulation by chemical, physical, or biological stimuli, can prove to be problematic because it can lead to the development of persistent inflammation [52].

CRP, which is a factor that predicts inflammation levels, did not change in our animal model (data not shown). No systemic inflammatory response was

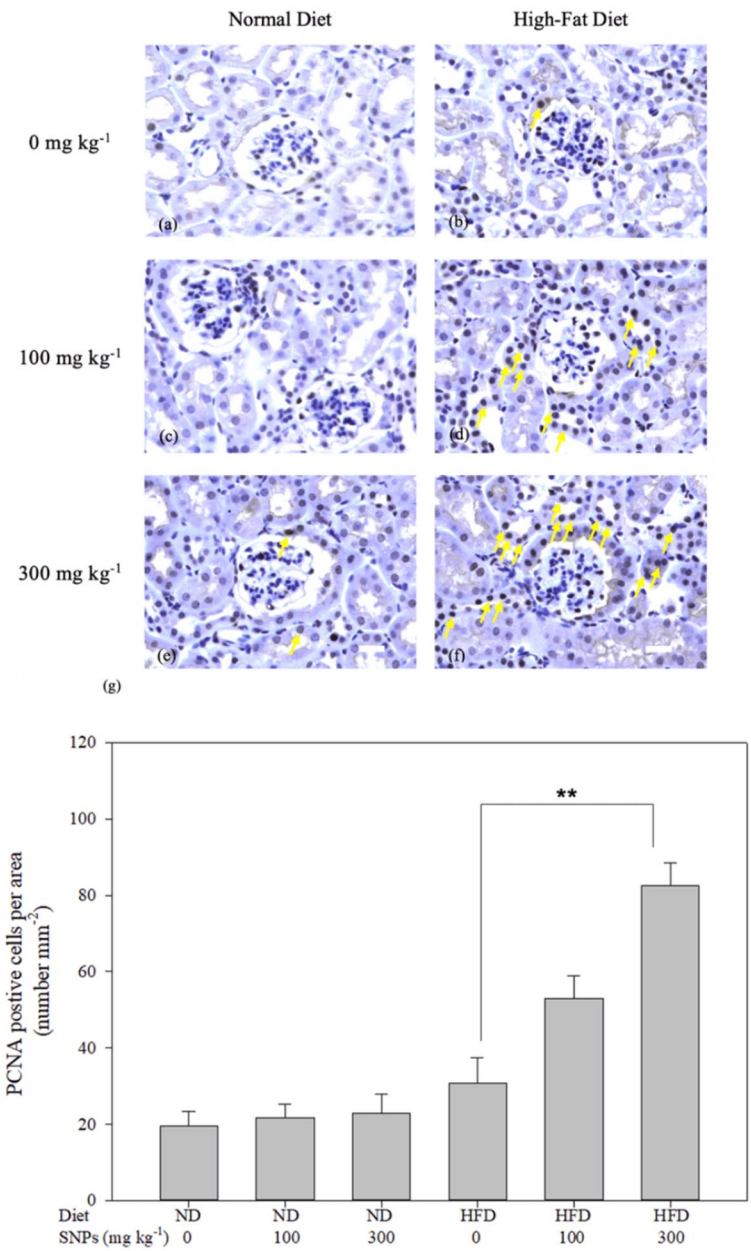

Fig. 5 Level of PCNA detected by using immunohistochemical staining. Mice were fed the ND (**a**, **c** and **e**) or HFD (**b**, **d** and **f**) for 25 weeks and treated with 0 (**a**, **b**), 100 (**c**, **d**), or 300 (**e**, **f**) mg of SNPs kg^{-1} body weight twice per week. The scale bars represent 100 μm (**a**–**f**). The percentage of PCNA-positive cells was analyzed using Image-Pro (**g**). The data are presented as the means ± standard errors of the means ($n = 6$)

observed in our mouse model. Hence, to understand chronic inflammation in our experimental model, the levels of cytokines, including IL-6, TNF-α, and TGF-β, were analyzed by IHC. IHC staining revealed no significant changes in IL-6 or TNF-α expression in the ND groups treated or not treated with SNPs (Figs. 6a, c, e, 7a, c and e); nevertheless, IL-6 and TNF-α expression was increased in the HFD-SNP100 and HFD-SNP300 groups compared with the HFD-SNP0 group (Figs. 6b, d, f, 7b, d and f). IHC quantitative data ($p < 0.01$–0.001, ANOVA) (Figs. 6g and 7g) demonstrated that the IL-6 and TNF-α expression was induced in the HFD-SNP100 and HFD-SNP300 groups compared with the HFD-SNP0 group. However, TGF-β expression was not activated in our animal model ($p > 0.05$, ANOVA) (Figs. S3a–g).

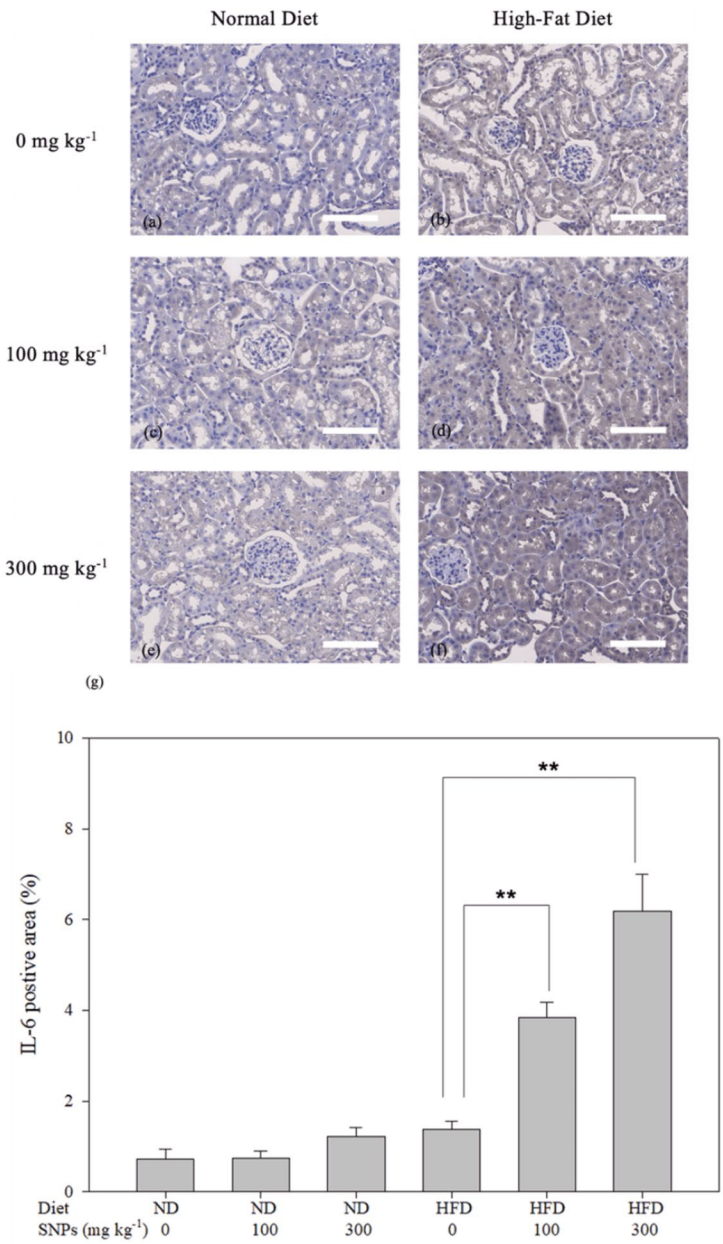

Fig. 6 The level of IL-6 was determined by immunohistochemical staining. Mice were fed the ND (**a**, **c** and **e**) or HFD (**b**, **d** and **f**) for 25 weeks and treated with 0 (**a**, **b**), 100 (**c**, **d**), or 300 (**e**, **f**) mg of SNPs kg^{-1} body weight twice per week. The scale bars represent 100 μm (**a**–**f**). The percentage of positive IL-6 staining/area was analyzed using Image-Pro (**g**). The data are presented as the means ± standard errors of the means ($n = 6$)

In kidney disease, IL-6 is related to proinflammatory actions such as B-cell stimulation [54, 55], the estimated glomerular filtration rate [56], and atherosclerosis [57]. Hence, IL-6 expression not only induces inflammation but also affects kidney function. Another possible role of IL-6 is increasing the transcription level of fibroblast growth factor 23 (FGF23), which regulates the phosphate homeostasis in the kidney, and this finding suggests that phosphate is excreted in the urine [58, 59]. Therefore, IL-6 plays an important role in CKD.

The cytokine TNF-α is released by immunologic cells such as monocytes and macrophages and is associated with several known functions: the control of cell death, inflammation, and the control of adaptive immunity [60, 61]. One of the possible ways TNF-α can act on CKD is by increasing the FGF23 levels, which causes mineral and

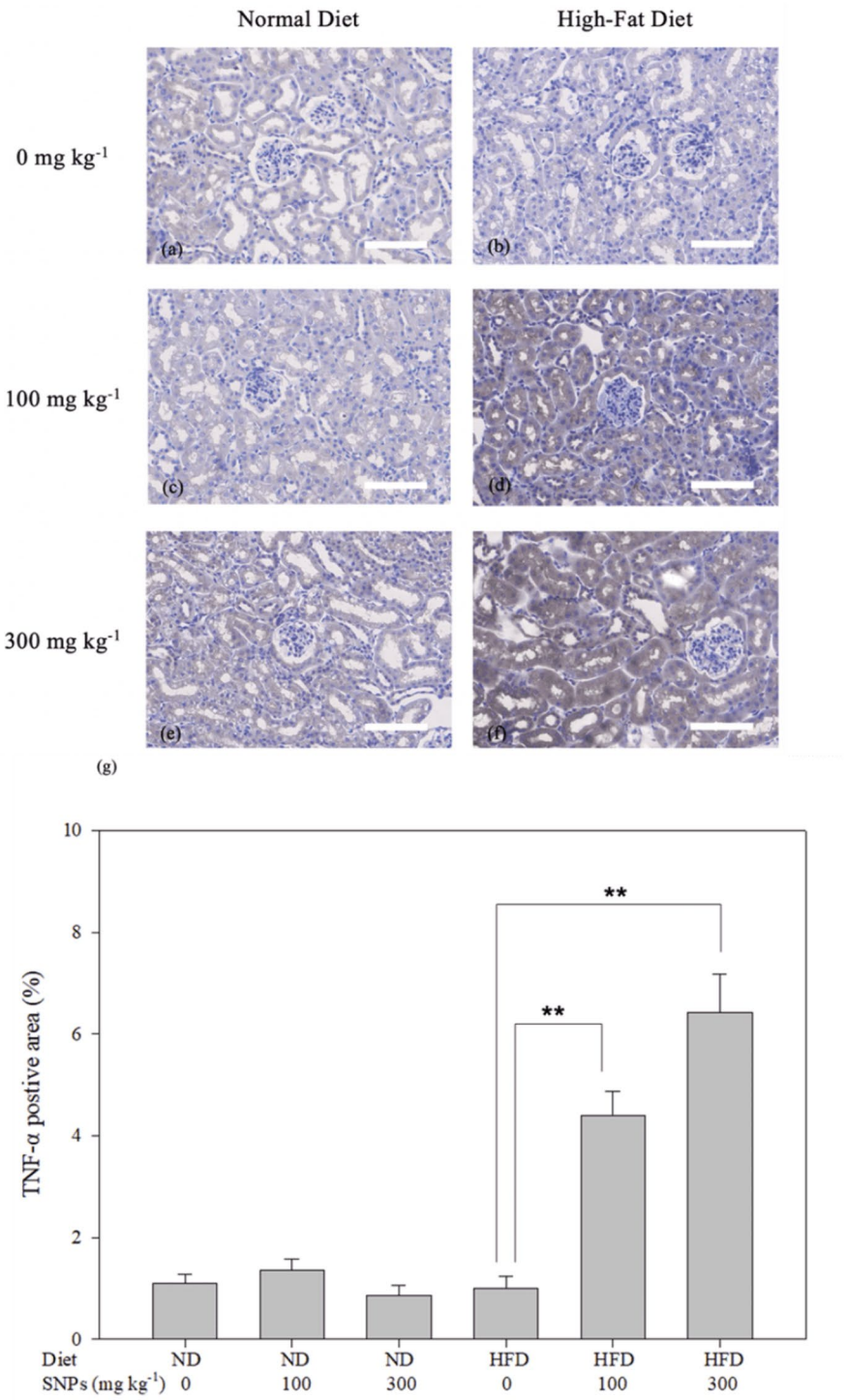

Fig. 7 The level of TNF-α was determined by immunohistochemical staining. Mice were fed the ND (**a**, **c** and **e**) or HFD (**b**, **d** and **f**) for 25 weeks and treated with 0 (**a**, **b**), 100 (**c**, **d**), or 300 (**e**, **f**) mg of SNPs kg^{-1} body weight twice per week. The scale bars represent 100 μm (**a**–**f**). The percentage of TNF-α positive cells/area was determined using Image-Pro (**g**). The data are presented as the means ± standard errors of the means ($n = 6$)

bone disorders and is related to the mortality of CKD patients [62]. A mice study has revealed that TNF-α confers kidney protection via macrophage recruitment, histopathological changes, a reduction in the serum creatinine level, and albuminuria in the kidneys [63]. Therefore, the risk of exposure to SNPs associated with

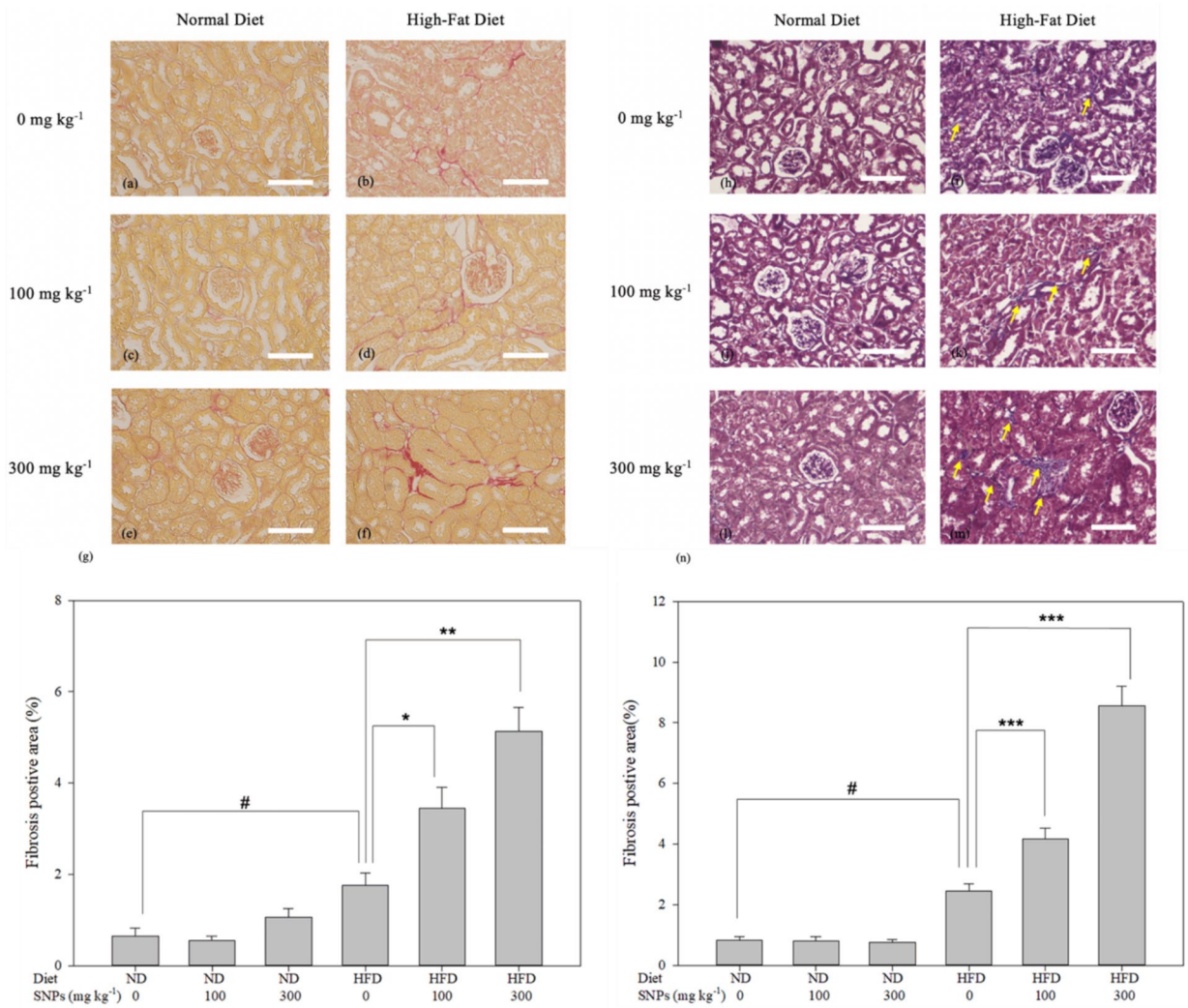

Fig. 8 The degree of fibrosis was observed by picrosirius red staining (**a**–**f**) and the Masson's Trichrome stain (**h**–**m**). Mice were fed the ND (**a**, **c**, **e**, **h**, **j** and **l**) or HFD (**b**, **d**, **f**, **i**, **k** and **m**) for 25 weeks and treated with 0 (**a**, **b**, **h** and **i**), 100 (**c**, **d**, **j** and **k**), or 300 (**e**, **f**, **l** and **m**) mg of SNPs kg^{-1} body weight twice per week. The arrow indicates positive picrosirius red staining. #, $p < 0.001$ for the comparison of the HFD-SNP0 group with the ND-SNP0 group, as revealed by ANOVA. The scale bars represent 100 μm (**a**–**f**, **h**–**m**). The degree of fibrosis was quantified using Image-Pro (**g**, **n**). The data are expressed as the means ± standard errors of the means ($n = 6$)

modern dietary habits provides important experimental evidence for evaluating the safety of SNPs, especially with regard to human health.

3.6 Increased fibrosis and oxidative stress through 4-HNE in the mouse model

Picrosirius red staining and fibrosis quantitative data showed that kidney fibrosis was induced in the HFD-SNP0 group compared with the ND-SNP0 group, which illustrated that an HFD could increase the fibrosis in the kidney ($p < 0.05$, ANOVA) (Fig. 8a, b, and g). ND-SNP100 and ND-SNP300 showed no positive staining (Fig. 8c and e). In the HFD groups, kidney fibrosis was increased in a dose-dependent manner in the mice fed increasing doses of SNPs ($p < 0.05$–0.01, ANOVA) (Fig. 8b, d, f and g). Similarly, kidney fibrosis was also observed by Mason's trichrome staining and quantitative analysis ($p < 0.001$, ANOVA) (Fig. 8h–n). In ND groups, no positive 4-HNE staining, an oxidative stress marker, was observed (Fig. 9a, c and e). Among the mice continuously fed the HFD and treated with SNPs, the expression of 4-HNE was increased in the HFD-SNP100 and HFD-SNP300 groups compared with the HFD-SNP0 group, as revealed by IHC staining and quantitative analysis ($p < 0.001$, ANOVA) (Fig. 9b, d, f and g).

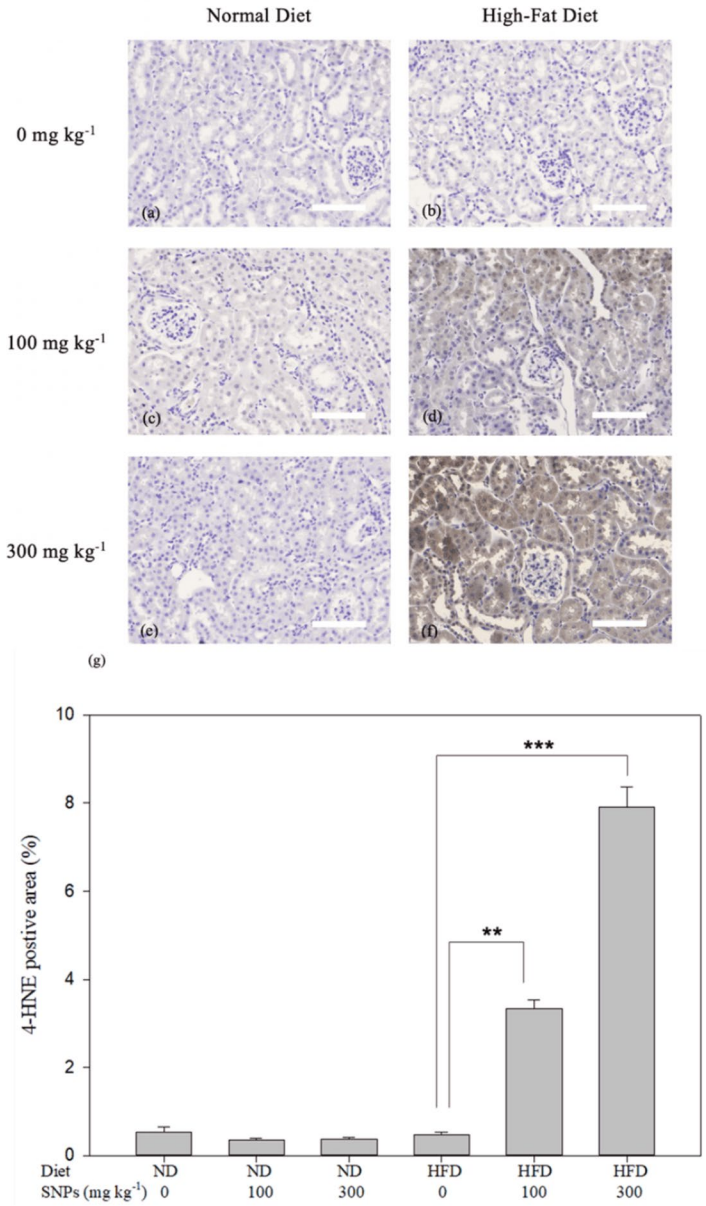

Fig. 9 The degree of oxidative stress was determined by immunohistochemical staining for 4-HNE. Mice were fed the ND (**a**, **c** and **e**) or HFD (**b**, **d** and **f**) for 25 weeks and treated with 0 (**a**, **b**), 100 (**c**, **d**), or 300 (**e**, **f**) mg of SNPs kg^{-1} body weight twice per week. The scale bars represent 100 μm (**a**–**f**). The percentage of positive 4-HNE staining/area was analyzed using Image-Pro (**g**). The data are presented as the means ± standard errors of the means ($n = 6$)

A diverse array of stressors, such as reactive oxygen species (ROS), DNA damage, mitochondrial dysfunction, nephrotoxins, mechanical stress, and oxidative stress, can induce kidney fibrosis [64]. Various stressors induce kidney fibrosis via different signaling pathways and increase senescence-associated secretory phenotype expression, which leads to fibroblast activation, abnormal extracellular matrix accumulation, and renal fibrosis [64, 65]. Signaling pathways such as the TGF-β and 4-HNE pathways participate in oxidative stress, suggesting kidney injury and fibrosis. One of the key controlling factors appears to be TGF-β which induces fibrosis via the action of TGF-β/Mathers against decapentaplegic homolog 3 [66, 67]. The peroxidation of fatty acids elevates the production of 4-HNE, which induces ROS, inflammation, apoptosis, and fibrosis [68–70]. In our study, the induction of renal fibrosis may have occurred as a result of increased 4-HNE expression but

not elevated TGF-β expression; however, the underlying mechanism remains unknown.

In this study, we demonstrated that the combination of long-term HFD and the administration of SNPs can induce kidney injury in the ICR mice. Our data showed that 25 weeks of HFD consumption and SNP treatment via feeding induced abnormal lipid accumulation in the kidney, which is consistent with previous findings [4]. Additionally, the manifestations of kidney injury in HFD-fed and administered SNP mice included tubular basophilia, basement membrane thickening, immune cell infiltration, an increased number of abnormal renal parenchyma, and prominent hyaline casts; moreover, the pathological consequences revealed kidney malfunction.

Previous studies found that HFD and SNPs affect kidney organs. For example, lipogenic enzymes are stimulated by an HFD and inhibit lipolysis; therefore, excess lipids within the kidney alter the metabolism of lipids and lead to glomerulosclerosis, interstitial fibrosis, and albuminuria [49]. Lipotoxic effects induced via the accumulation of lipids are reflected by oxidative stress, mitochondrial fission, and lipid metabolism dysfunction [4, 7]. Yamamoto et al. reported that kidney injury was induced by the accumulation of phospholipids in lysosomes within renal proximal tubular cells [6]. Sasai et al. reported that SNPs caused kidney damage with tubular injury and inflammation in rats and that these effects persisted even after the rats were no longer exposed to SNPs [34]. CKD is presumed to be due to possible environmental toxins, including water and food-related toxins and element exposure, such as lead, chromium, and silica [71–73]. Therefore, it appears that an HFD and SNPs can cause the same result: kidney injury formation.

Activating transcription factor 3 (ATF3) was upregulated in cells treated with SNPs and was also detected through a cDNA array [22]. ATF3 is a transcription factor that plays a key role in the regulation of apoptosis, oncogenesis, inflammation, and DNA repair. This transcription factor enhances hepatic triglyceride hydrolysis, intestinal lipid absorption, and fatty acid oxidation [74]. Therefore, ATF3 was proposed to be a target molecule involved in steatosis. Lee et al. [75] used global proteomics to study SNP-induced mechanisms. Most proteins induced by SNP treatment are involved in lipid metabolism, and the expression of genes encoding sphingolipid delta(4)-desaturase DES1, lysophospholipid acyltransferase 7, neutral cholesterol ester hydrolase 1, choline transporter-like protein 1, microsomal glutathione S-transferase 3, medium-chain specific acyl-CoA dehydrogenase mitochondrial and glycosylphosphatidylinositol anchor attachment 1 protein, was significantly upregulated [75]; these results are consistent with the increased TG levels detected in our mouse model. The evidence showed that SNPs are strongly associated with lipid metabolism; however, the mechanism through which SNPs induce lipid metabolism remains unclear.

A modern diet rich in fats is believed to be a major factor affecting the development of fatty liver, obesity, and overweight worldwide, and obesity has been recognized as a key risk factor for the development of CKD [7, 76]. Our study identified SNPs as another important factor in the development of kidney injury in HFD-fed individuals. Hence, in addition to carefully controlling dietary or molecular contents, removing NPs, such as SNPs, can lead to diabetes, hypertension, fatty liver, obesity, and overweight [18, 77, 78], and these particles might also be therapeutic targets for preventing CKD formation.

The study has several limitations. Although our results suggest that SNPs are major drivers of renal injury, we did not directly elucidate the detailed biological mechanism induced by these SNPs. Moreover, the parameters used to define kidney injury in our mouse model may differ from the glomerular filtration rate, which is used in clinical settings. The HFD used in this study was not the same as the modern or Western diets consumed by humans. We may need to keep this fact in mind when evaluating our conclusion.

4 Conclusions

A mouse model was generated by treatment with SNPs and HFD, which mimic the SNPs in drinking water and modern dietary habits. Analyses of the body weight, kidney tissue histology, blood biochemistry assays, picrosirius red staining, quantitative RT-PCR, and immunohistochemical staining were used to assess the effects of the administration of different concentrations of SNPs (100 and 300 mg of SNP kg^{-1} mouse body weight) over 25 weeks. The results showed that the body weight did not change in either the ND- or HFD-fed mice administered SNPs. During the experimental period, no abnormal animal behaviors or clinical signs were observed by the naked eye in our mouse model. The accumulation of silicon and TGs was observed and might be related to renal injury in the mice administered SNPs and fed the HFD. Biochemical blood assays, H&E morphology observations, and CKD markers revealed that increased serum levels of BUN, CRE, and UA and induced mRNA levels of *Lcn 2*, *Kim-1*, and *Vim* also confirmed kidney dysfunction in the mice administered SNPs and fed the HFD. Increased local inflammation, renal fibrosis, and oxidative stress, as indicated by IHC for IL-6, TNF-α, 4-HNE, and by picrosirius red and mason trichrome staining for fibrosis. Based on the results of our study, the long-term effect of SNPs in drinking water may represent a

hazard to kidney function in the setting of modern dietary habits.

In our experimental model, the induction of CKD was observed. Hence, our results illustrate the combined effect of modern dietary habits and SNPs provide important experimental evidence for the safety evaluation of SNPs, especially in human health. However, the mechanism of CKD remains unclear; nevertheless, oxidative stress was observed in our model. Our studies showed that renal damage is accelerated by an HFD and SNP treatment because SNPs, which are soldiers hidden in a Trojan horse, are a risk factor. The accumulation of SNPs could transform the metabolic confusion in kidney cells. To prevent the effects of SNPs on humans, long-term monitoring of the accumulation of SNPs in our environment is required. The influence of SNPs cannot be ignored, and we need to prevent the increases in potential risks during daily life.

Supplementary Information

The online version contains supplementary material available at https://doi.org/10.1186/s42834-025-00240-6.

Supplementary Material 1.

Acknowledgements
We thank the Taiwan Mouse Clinic, Academia Sinica, and Taiwan Animal Consortium for technical support in mouse sacrifice, H&E staining, blood biochemistry assays, and immunohistochemistry.

Authors' contributions
Tzung Cheng Ye: Conceptualization, writing—original draft, investigation, visualization. Shu-Ju Chao: Conceptualization. Chihpin Huang: Conceptualization, supervision, resources. All authors have read and agreed to the published version of the manuscript.

Funding
Funding agency: Ministry of Science and Technology Taiwan. Grant number: MOST 108-2221-E-009-074-MY3. Animal study ethics approval from National Yang Ming Chao Tung University (National Chao Tung University). Approval number: NCTU-IACUC-107052.

Data availability
The data that supports the findings of this study are available within the article.

Declarations

Competing interests
The authors declare they have no competing interests.

Received: 10 May 2024 Accepted: 22 January 2025
Published online: 19 February 2025

References

1. Camara NOS, Iseki K, Kramer H, Liu ZH, Sharma K. Kidney disease and obesity: epidemiology, mechanisms and treatment. Nat Rev Nephrol. 2017;13:181–90.
2. Kassi E, Pervanidou P, Kaltsas G, Chrousos G. Metabolic syndrome: definitions and controversies. BMC Med. 2011;9:48.
3. Gancheva S, Jelenik T, Alvarez-Hernandez E, Roden M. Interorgan metabolic crosstalk in human insulin resistance. Physiol Rev. 2018;98:1371–415.
4. Chen Y, Deb DK, Fu X, Yi B, Liang Y, Du J, et al. ATP-citrate lyase is an epigenetic regulator to promote obesity-related kidney injury. FASEB J. 2019;33:9602–15.
5. de Vries AP, Ruggenenti P, Ruan XZ, Praga M, Cruzado JM, Bajema IM, et al. Fatty kidney: emerging role of ectopic lipid in obesity-related renal disease. Lancet Diabetes Endo. 2014;2:417–26.
6. Yamamoto T, Takabatake Y, Takahashi A, Kimura T, Namba T, Matsuda J, et al. High-fat diet-induced lysosomal dysfunction and impaired autophagic flux contribute to lipotoxicity in the kidney. J Am Soc Nephrol. 2017;28:1534–51.
7. Sun Y, Ge X, Li X, He J, Wei X, Du J, et al. High-fat diet promotes renal injury by inducing oxidative stress and mitochondrial dysfunction. Cell Death Dis. 2020;11:914.
8. Jayasumana C, Orantes C, Herrera R, Almaguer M, Lopez L, Silva LC, et al. Chronic interstitial nephritis in agricultural communities: a worldwide epidemic with social, occupational and environmental determinants. Nephrol Dial Transpl. 2017;32:234–41.
9. Vervaet BA, Nast CC, Jayasumana C, Schreurs G, Roels F, Herath C, et al. Chronic interstitial nephritis in agricultural communities is a toxin-induced proximal tubular nephropathy. Kidney Int. 2020;97:350–69.
10. Sousa VS, Ribau Teixeira M. Metal-based engineered nanoparticles in the drinking water treatment systems: A critical review. Sci Total Environ. 2020;707:136077.
11. Roshanfekrnahzomi Z, Badpa P, Esfandiari B, Taheri S, Nouri M, Akhtari K, et al. Silica nanoparticles induce conformational changes of tau protein and oxidative stress and apoptosis in neuroblastoma cell line. Int J Biol Macromol. 2019;124:1312–20.
12. Deciga-Alcaraz A, Medina-Reyes EI, Delgado-Buenrostro NL, Rodriguez-Ibarra C, Ganem-Rondero A, Vazquez-Zapien GJ, et al. Toxicity of engineered nanomaterials with different physicochemical properties and the role of protein corona on cellular uptake and intrinsic ROS production. Toxicology. 2020;442:152545.
13. Cheng Y, Chen Z, Yang S, Liu T, Yin L, Pu Y, et al. Nanomaterials-induced toxicity on cardiac myocytes and tissues, and emerging toxicity assessment techniques. Sci Total Environ. 2021;800:149584.
14. Almansour M, Alarifi S, Jarrar B. In vivo investigation on the chronic hepatotoxicity induced by intraperitoneal administration of 10-nm silicon dioxide nanoparticles. Int J Nanomed. 2018;13:2685–96.
15. Li X, Li Y, Lv S, Xu H, Ma R, Sun Z, et al. Long-term respiratory exposure to amorphous silica nanoparticles promoted systemic inflammation and progression of fibrosis in a susceptible mouse model. Chemosphere. 2022;300:134633.
16. Guilloteau E, Djouina M, Caboche S, Waxin C, Deboudt K, Beury D, et al. Exposure to atmospheric Ag, TiO_2, Ti and SiO_2 engineered nanoparticles modulates gut inflammatory response and microbiota in mice. Ecotox Environ Safe. 2022;236:113442.
17. He H, Zhou Y, Liu L, Cui J, Pei Y, Cao J, et al. Bioinformatics analysis reveals lipid metabolism may play an important role in the SiO_2-stimulated rat model. Cell Signal. 2023;108:110716.
18. Yu Y, Duan J, Li Y, Li Y, Jing L, Yang M, et al. Silica nanoparticles induce liver fibrosis via TGF-β_1/Smad3 pathway in ICR mice. Int J Nanomed. 2017;12:6045–57.
19. Abdel-Latif HMR, Shukry M, El Euony OI, Mohamed Soliman M, Noreldin AE, Ghetas HA, et al. Hazardous effects of SiO_2 nanoparticles on liver and kidney functions, histopathological characteristics, and transcriptomic responses in Nile tilapia (*Oreochromis niloticus*) juveniles. Biology. 2021;10:183.
20. Huang FC, Du Y, Zhang XF, Guan L, Liu XM, Zeng M. SiO_2 dust induces inflammation and pulmonary fibrosis in rat lungs through activation of ASMase/ceramide pathway. J Appl Toxicol. 2023;43:1319–31.
21. Gong C, Tao G, Yang L, Liu J, Liu Q, Zhuang Z. SiO_2 nanoparticles induce global genomic hypomethylation in HaCaT cells. Biochem Bioph Res Co. 2010;397:397–400.
22. Schmitz C, Welck J, Tavernaro I, Grinberg M, Rahnenführer J, Kiemer AK, et al. Mechanical strain mimicking breathing amplifies alterations in gene expression induced by SiO_2 NPs in lung epithelial cells. Nanotoxicology. 2019;13:1227–43.

23. Yang X, Liu J, He H, Zhou L, Gong C, Wang X, et al. SiO_2 nanoparticles induce cytotoxicity and protein expression alteration in HaCaT cells. Part Fibre Toxicol. 2010;7:1.
24. Khan I, Saeed K, Khan I. Nanoparticles: Properties, applications and toxicities. Arab J Chem. 2019;12:908–31.
25. Mascarenhas S, Mutnuri S, Ganguly A. Deleterious role of trace elements – Silica and lead in the development of chronic kidney disease. Chemosphere. 2017;177:239–49.
26. Nikagolla C, Meredith KT, Dawes LA, Banati RB, Millar GJ. Using water quality and isotope studies to inform research in chronic kidney disease of unknown aetiology endemic areas in Sri Lanka. Sci Total Environ. 2020;745:140896.
27. Boudard D, Aureli F, Laurent B, Sturm N, Raggi A, Antier E, et al. Chronic oral exposure to synthetic amorphous silica (NM-200) results in renal and liver lesions in mice. Kidney Int Rep. 2019;4:1463–71.
28. Chan WT, Liu CC, Chiang Chiau JS, Tsai ST, Liang CK, Cheng ML, et al. In vivo toxicologic study of larger silica nanoparticles in mice. Int J Nanomed. 2017;12:3421–32.
29. Hassankhani R, Esmaeillou M, Tehrani AA, Nasirzadeh K, Khadir F, Maadi H. In vivo toxicity of orally administrated silicon dioxide nanoparticles in healthy adult mice. Environ Sci Pollut R. 2015;22:1127–32.
30. Yu Y, Li Y, Wang W, Jin M, Du Z, Li Y, et al. Acute Toxicity of amorphous silica nanoparticles in intravenously exposed ICR Mice. PLoS One. 2013;8:e61346.
31. Murugadoss S, Lison D, Godderis L, Van Den Brule S, Mast J, Brassinne F, et al. Toxicology of silica nanoparticles: an update. Arch Toxicol. 2017;91:2967–3010.
32. Cabellos J, Gimeno-Benito I, Catalan J, Lindberg HK, Vales G, Fernandez-Rosas E, et al. Short-term oral administration of non-porous and mesoporous silica did not induce local or systemic toxicity in mice. Nanotoxicology. 2020;14:1324–41.
33. Kawakami K, Takeshita A, Furushima K, Miyajima M, Hatamura I, Kuro-o M, et al. Persistent fibroblast growth factor 23 signalling in the parathyroid glands for secondary hyperparathyroidism in mice with chronic kidney disease. Sci Rep. 2017;7:40534.
34. Sasai F, Rogers KL, Orlicky DJ, Stem A, Schaeffer J, Garcia G, et al. Inhaled silica nanoparticles cause chronic kidney disease in rats. Am J Physiol Renal. 2022;323:F48–58.
35. Manzanares D, Cena V. Endocytosis: the nanoparticle and submicron nanocompounds gateway into the cell. Pharmaceutics. 2020;12:371.
36. Shen J, Zhang J, Wen J, Ming Q, Zhang J, Xu Y. Correlation of serum alanine aminotransferase and aspartate aminotransferase with coronary heart disease. Int J Clin Exp Med. 2015;8:4399–404.
37. Raurich JM, Llompart-Pou JA, Rodriguez-Yago M, Ferreruela M, Royo C, Ayestarán I. Role of elevated aminotransferases in ICU patients with rhabdomyolysis. Am Surgeon. 2015;81:1209–15.
38. Weng SF, Kai J, Guha IN, Qureshi N. The value of aspartate aminotransferase and alanine aminotransferase in cardiovascular disease risk assessment. Open Heart. 2015;2:e000272.
39. Askari H, Seifi B, Kadkhodaee M. Evaluation of renal-hepatic functional indices and blood pressure based on the progress of time in a rat model of chronic kidney disease. Nephro-Urol Mon. 2016;8:e37840.
40. Teixido-Trujillo S, Luis-Lima S, Lopez-Martinez M, Navarro-Diaz M, Diaz-Martin L, Escasany-Martinez E, et al. Measured GFR in murine animal models: review on methods, techniques, and procedures. Pflugers Arch Eur J Physiol. 2023;475:1241–50.
41. Hinojosa-Laborde C, Jespersen B, Shade R. Physiology lab demonstration: glomerular filtration rate in a rat. JoVE-J Vis Exp. 2015;101:e52425.
42. Serfilippi LM, Pallman DR, Russell B. Serum clinical chemistry and hematology reference values in outbred stocks of albino mice from three commonly used vendors and two inbred strains of albino mice. Contemp Top Lab Anim. 2003;42:46-52.
43. Cao YH, Lv LL, Zhang X, Hu H, Ding LH, Yin D, et al. Urinary vimentin mRNA as a potential novel biomarker of renal fibrosis. Am J Physiol-Renal. 2015;309:F514–22.
44. Bhavsar NA, Kottgen A, Coresh J, Astor BC. Neutrophil gelatinase-associated lipocalin (NGAL) and kidney injury molecule 1 (KIM-1) as predictors of incident CKD stage 3: the Atherosclerosis Risk in Communities (ARIC) Study. Am J Kidney Dis. 2012;60:233–40.
45. Hard GC, Khan KN. A contemporary overview of chronic progressive nephropathy in the laboratory rat, and its significance for human risk assessment. Toxicol Pathol. 2004;32:171–80.
46. Decleves AE, Mathew AV, Cunard R, Sharma K. AMPK mediates the initiation of kidney disease induced by a high-fat diet. J Am Soc Nephrol. 2011;22:1846–55.
47. Juszczak F, Caron N, Mathew AV, Decleves AE. Critical role for AMPK in metabolic disease-induced chronic kidney disease. Int J Mol Sci. 2020;21:7994.
48. Rodriguez C, Sanchez A, Saenz-Medina J, Munoz M, Hernandez M, Lopez M, et al. Activation of AMP kinase ameliorates kidney vascular dysfunction, oxidative stress and inflammation in rodent models of obesity. Brit J Pharmacol. 2021;178:4085–103.
49. Kume S, Uzu T, Araki S, Sugimoto T, Isshiki K, Chin-Kanasaki M, et al. Role of altered renal lipid metabolism in the development of renal injury induced by a high-fat diet. J Am Soc Nephrol. 2007;18:2715–23.
50. Hard GC. Mechanisms of chemically induced renal carcinogenesis in the laboratory rodent. Toxicol Pathol. 1998;26:104–12.
51. Schmitt R, Melk A. Molecular mechanisms of renal aging. Kidney Int. 2017;92:569–79.
52. Germolec DR, Shipkowski KA, Frawley RP, Evans E. Markers of Inflammation. In: DeWitt JC, Rockwell CE, Bowman CC, editors. Immunotoxicity Testing: Methods and Protocols. New York: Springer New York; 2018. p. 57–79.
53. Petreski T, Piko N, Ekart R, Hojs R, Bevc S. Review on inflammation markers in chronic kidney disease. Biomedicines. 2021;9:182.
54. Rose-John S. Interleukin-6 family cytokines. CSH Perspect Biol. 2018;10:a028415.
55. Scheller J, Chalaris A, Schmidt-Arras D, Rose-John S. The pro- and anti-inflammatory properties of the cytokine interleukin-6. BBA-Mol Cell Res. 2011;1813:878–88.
56. Amdur RL, Feldman HI, Gupta J, Yang W, Kanetsky P, Shlipak M, et al. Inflammation and progression of CKD: the CRIC study. Clin J Am Soc Nephro. 2016;11:1546–56.
57. Desjardins MP, Sidibe A, Fortier C, Mac-Way F, Marquis K, De Serres S, et al. Association of interleukin-6 with aortic stiffness in end-stage renal disease. J Am Soc Hypertens. 2018;12:5–13.
58. Perwad F, Zhang MYH, Tenenhouse HS, Portale AA. Fibroblast growth factor 23 impairs phosphorus and vitamin D metabolism in vivo and suppresses 25-hydroxyvitamin D-1α-hydroxylase expression in vitro. Am J Physiol-Renal. 2007;293:F1577–83.
59. Fukumoto S. Physiological regulation and disorders of phosphate metabolism: pivotal role of fibroblast growth factor 23. Internal Med. 2008;47:337–43.
60. Vanamee ES, Faustman DL. Structural principles of tumor necrosis factor superfamily signaling. Sci Signal. 2018;11:eaao4910.
61. Wallach D. The tumor necrosis factor family: family conventions and private idiosyncrasies. CSH Perspect Biol. 2018;10:a028431.
62. Egli-Spichtig D, Imenez Silva PH, Glaudemans B, Gehring N, Bettoni C, Zhang MYH, et al. Tumor necrosis factor stimulates fibroblast growth factor 23 levels in chronic kidney disease and non-renal inflammation. Kidney Int. 2019;96:890–905.
63. Awad AS, You H, Gao T, Cooper TK, Nedospasov SA, Vacher J, et al. Macrophage-derived tumor necrosis factor-α mediates diabetic renal injury. Kidney Int. 2015;88:722–33.
64. Xu J, Zhou L, Liu Y. Cellular senescence in kidney fibrosis: pathologic significance and therapeutic strategies. Front Pharmacol. 2020;11:601325.
65. Wang WJ, Chen XM, Cai GY. Cellular senescence and the senescence-associated secretory phenotype: Potential therapeutic targets for renal fibrosis. Exp Gerontol. 2021;151:111403.
66. Sun YBY, Qu X, Caruana G, Li J. The origin of renal fibroblasts/myofibroblasts and the signals that trigger fibrosis. Differentiation. 2016;92:102–7.
67. Higgins SP, Tang Y, Higgins CE, Mian B, Zhang W, Czekay RP, et al. TGF-β1/p53 signaling in renal fibrogenesis. Cell Signal. 2018;43:1–10.
68. Allen CE, Sanders PW. Hypertensive nephrosclerosis: not enough of a good thing? Am J Physiol-Renal. 2013;304:F674–5.
69. Jaganjac M, Milkovic L, Gegotek A, Cindric M, Zarkovic K, Skrzydlewska E, et al. The relevance of pathophysiological alterations in redox signaling of 4-hydroxynonenal for pharmacological therapies of major stress-associated diseases. Free Radical Bio Med. 2020;157:128–53.

70. Uddin MJ, Kim EH, Hannan MA, Ha H. Pharmacotherapy against oxidative stress in chronic kidney disease: promising small molecule natural products targeting Nrf2-HO-1 signaling. Antioxidants. 2021;10:258.
71. Brewster UC. Chronic kidney disease from environmental and occupational toxins. Conn Med. 2006;70:229–37.
72. Ghahramani N. Silica nephropathy. Int J Occup Env Med. 2010;1:108–15.
73. Fowler BA. Mechanisms of kidney cell injury from metals. Environ Health Persp. 1993;100:57–63.
74. Hu S, Zhao X, Li R, Hu C, Wu H, Li J, et al. Activating transcription factor 3, glucolipid metabolism, and metabolic diseases. J Mol Cell Biol. 2022;14: mjac067.
75. Lee SY, Kim IY, Heo MB, Moon JH, Son JG, Lee TG. Global proteomics to study silica nanoparticle-induced cytotoxicity and its mechanisms in HepG2 cells. Biomolecules. 2021;11:375.
76. Chen S, Chen J, Li S, Guo F, Li A, Wu H, et al. High-fat diet-induced renal proximal tubular inflammatory injury: an emerging risk factor of chronic kidney disease. Front Physiol. 2021;12:786599.
77. Zuo D, Duan Z, Jia Y, Chu T, He Q, Yuan J, et al. Amphipathic silica nanoparticles induce cytotoxicity through oxidative stress mediated and p53 dependent apoptosis pathway in human liver cell line HL-7702 and rat liver cell line BRL-3A. Colloid Surface B. 2016;145:232–40.
78. Petrick L, Rosenblat M, Paland N, Aviram M. Silicon dioxide nanoparticles increase macrophage atherogenicity: Stimulation of cellular cytotoxicity, oxidative stress, and triglycerides accumulation. Environ Toxicol. 2016;31:713–23.

Publisher's Note